

AAA⁺ Chaperone ClpX Regulates Dynamics of Prokaryotic Cytoskeletal Protein FtsZ^{*[5]}

Received for publication, October 29, 2009, and in revised form, December 4, 2009. Published, JBC Papers in Press, December 18, 2009, DOI 10.1074/jbc.M109.080739

Shinya Sugimoto^{†1}, Kunitoshi Yamanaka[‡], Shingo Nishikori[‡], Atsushi Miyagi^{§¶}, Toshio Ando[§], and Teru Ogura^{‡2}

From the [†]Department of Molecular Cell Biology, Institute of Molecular Embryology and Genetics, Kumamoto University, 2-2-1 Honjo, Kumamoto 860-0811, the [‡]Department of Physics, Kanazawa University, Kakuma-machi, Kanazawa 920-1192, and the [§]Takara-Bio Endowed Laboratory, Institute for Protein Research, Osaka University, 6-2-3 Furuedai, Suita, Osaka 565-0874, Japan

AAA⁺ chaperone ClpX has been suggested to be a modulator of prokaryotic cytoskeletal protein FtsZ, but the details of recognition and remodeling of FtsZ by ClpX are largely unknown. In this study, we have extensively investigated the nature of FtsZ polymers and mechanisms of ClpX-regulated FtsZ polymer dynamics. We found that FtsZ polymerization is inhibited by ClpX in an ATP-independent manner and that the N-terminal domain of ClpX plays a crucial role for the inhibition of FtsZ polymerization. Single molecule analysis with high speed atomic force microscopy directly revealed that FtsZ polymer is in a dynamic equilibrium between polymerization and depolymerization on a time scale of several seconds. ClpX disassembles FtsZ polymers presumably by blocking reassembly of FtsZ. Furthermore, *Escherichia coli* cells overproducing ClpX and N-terminal domain of ClpX show filamentous morphology with abnormal localization of FtsZ. These data together suggest that ClpX modulates FtsZ polymer dynamics in an ATP-independent fashion, which is achieved by interaction between the N-terminal domain of ClpX and FtsZ monomers or oligomers.

ClpX is a member of the Clp/Hsp100 class of AAA⁺ (ATPases associated with diverse cellular activities) family proteins (1). A hallmark of the AAA⁺ proteins is the formation of a hexameric ring structure with a central pore in an ATP-independent or -dependent manner. ClpX forms a complex with the tetradecameric protease component, ClpP, and the complex ClpXP degrades various cellular proteins (2). ClpX consists of an N-terminal domain and the following AAA⁺ domain. The N-terminal domain recognizes specific substrate proteins, whereas the AAA⁺ domain transmits energy of ATP to mechanical action like unfolding and translocation of substrate proteins (3). The N-terminal domain of ClpX is essential for degradation of some proteins, including MuA and λO, but not for the degradation of other substrate proteins, such as SsrA-tagged proteins (4). Furthermore, the N-terminal domain itself

forms a dimer and has a potential role in quality control of substrate proteins like general chaperones (4).

FtsZ, a structural homolog of the eukaryotic cytoskeleton protein tubulin, is an essential protein and plays a key role in bacterial cell division (5–7). FtsZ polymerizes into filaments by the head-to-tail association of individual protomers at mid-cell, which functions as the scaffold for assembly of at least a dozen cell division proteins, and a ring-like large protein complex (Z-ring) is subsequently formed. As in the case of tubulin, polymerization of FtsZ is triggered by the GTP binding (8–10). *In vitro*, FtsZ assembles into several polymeric forms such as single straight or curved filaments, bundles, and sheets, depending on the experimental conditions (8–14). The observation that the expression level of FtsZ is constant in cells at various growth phases suggests that Z-ring formation is primarily regulated at the level of FtsZ assembly. To date, several proteins regulating FtsZ dynamics have been identified (7). For example, in *Escherichia coli*, inner membrane proteins FtsA and ZipA collaborate in the anchoring of FtsZ to membrane and thus stabilize the Z-ring (15, 16). In contrast, MinC and SulA inhibit FtsZ assembly (17, 18).

By a proteomic approach, ~50 proteins, including FtsZ, have been identified as candidates of the ClpX substrate, but how ClpX recognizes FtsZ and the roles of ClpX in the fate of FtsZ are unclear (2). Recently, it has been reported that in *Bacillus subtilis* ClpX inhibits FtsZ polymerization *in vivo* and *in vitro* in an ATP-independent manner but does not degrade it (19, 20). However, molecular mechanisms of regulating FtsZ monomer-polymer dynamics are still largely unknown. More recently, it has been reported that in *E. coli* ClpX disassembles FtsZ polymers in cooperation with ClpP by degrading polymers preferentially rather than monomers and that ClpX revealed no significant activity to inhibit FtsZ polymerization (21). These controversial results might be accounted for by the difference in bacterial species and/or experimental conditions, but further studies are required to evaluate these differences.

In this study, using *E. coli* systems, we examined the nature of FtsZ polymers and roles of ClpX in regulation of FtsZ polymer dynamics. We demonstrated that high speed atomic force microscopy (AFM)³ is a superior method for visualizing FtsZ filament dynamics. ClpX significantly shifts FtsZ dynamic equi-

* This work was supported by a grant-in-aid for scientific research from the Japan Society for the Promotion of Science, by the Core Research for Evolutional Science and Technology program grant from the Japan Science and Technology Agency, and by grants from the Ministry of Education, Culture, Sports, Science and Technology of Japan.

[5] The on-line version of this article (available at <http://www.jbc.org>) contains supplemental Figs. S1–S5 and Table S1.

¹ Research Fellow of the Japan Society for the Promotion of Science.

² To whom correspondence should be addressed. Tel.: 81-96-373-6578; Fax: 81-96-373-6582; E-mail: ogura@gpo.kumamoto-u.ac.jp.

³ The abbreviations used are: AFM, atomic force microscopy; IPTG, isopropyl 1-thio-β-D-galactopyranoside; SEM, scanning electron microscopy; DAPI, 4,6-diamidino-2-phenylindole; ATPγS, adenosine 5'-O-(thiotriphosphate).

librium from polymer to monomer, and the N-terminal domain of ClpX has the potential activity to inhibit FtsZ polymerization. Based on our biochemical and cell biological evidence, we propose novel molecular mechanisms for remodeling of FtsZ polymer dynamics by ClpX.

EXPERIMENTAL PROCEDURES

Bacterial Strains and Plasmids—*E. coli* strains used in this study (supplemental Table S1) were grown at 37 °C in LB medium containing appropriate antibiotics (40 µg/ml kanamycin and 50 µg/ml ampicillin). The plasmids used in this study are also listed in supplemental Table S1. The *ftsZ* gene was amplified from *E. coli* JM109 and cloned into pET-15b (Novagen) and pGFP_{uv} (Clontech) plasmids using NdeI and BamHI restriction sites and SphI and XbaI restriction sites, respectively. The *ftsZΔC* encoding FtsZ residues 1–316, *clpX* encoding ClpX residues 1–424, *clpXΔN* encoding ClpX residues 61–424, *clpX-N* encoding ClpX residues 1–60 or *sspB* genes was also amplified from *E. coli* JM109 and cloned into pET-28b plasmid using NdeI and BamHI restriction sites. DNA fragment encoding the SsrA tag was cloned downstream of *gfp_{uv}* in pGFP_{uv}. DNA sequences of the cloned genes were confirmed.

Purification of Proteins—*E. coli* BL21(DE3) was transformed with pET15-FtsZ, pET28-FtsZΔC, pET28-ClpX, pET28-ClpXΔN, pET28-ClpX-N, pET28-SspB, and pGEX-ClpP (provided by Dr. S. Hishida) or pUHE-ClpB (provided by Dr. B. Bukau). *E. coli* KY2266 (22) was transformed with pGFP_{uv}-SsrA.

E. coli cells overproducing FtsZ or FtsZΔC were grown at 37 °C in LB medium containing 50 µg/ml ampicillin or 40 µg/ml kanamycin, respectively, and expression of the FtsZ variants was induced by the addition of isopropyl 1-thio-β-D-galactopyranoside (IPTG) (1 mM), followed by incubation at 37 °C for 3 h. Cells from 2 liters of culture were harvested by centrifugation and suspended in 100 ml of buffer A (20 mM Tris-HCl (pH 8.0), 400 mM NaCl, 20 mM imidazole, 10% (w/v) glycerol) supplemented with protease inhibitor mixture (Nakalai Tesque). After sonication on ice, cell lysates were centrifuged at 15,000 × *g* for 1 h at 4 °C, and the supernatant was loaded onto a HisTrap HP column (GE Healthcare). The column was washed with buffer A containing 50 mM imidazole, and recombinant proteins were then eluted using 50–500 mM imidazole gradient in buffer A. To remove contaminated GTP or GDP, eluted fractions were further purified by 35% ammonium sulfate precipitation and HiTrap DEAE column (GE Healthcare) chromatography using 0–500 mM NaCl gradient in buffer B (50 mM Tris-HCl (pH 8.0), 1 mM EDTA, 10% (w/v) glycerol). Each fraction containing FtsZ or FtsZΔC was stored separately at –80 °C.

E. coli cells overproducing ClpX, ClpXΔN, ClpX-N, or SspB were grown at 30 °C in LB medium containing 40 µg/ml kanamycin to an $A_{600} = 0.5$, and then IPTG was added to a final concentration of 0.1 mM. After an additional incubation for 2 h at 30 °C, cells were harvested and suspended in buffer C (50 mM Tris-HCl (pH 7.5), 100 mM KCl, 1 mM MgCl₂, 1 mM dithiothreitol, 20 mM imidazole, 0.01% Triton X-100, 10% (w/v) glycerol) supplemented with protease inhibitor mixture. After sonication on ice, cell lysates were centrifuged at 15,000 × *g* for 1 h at

4 °C, and the supernatant was loaded onto a HisTrap HP column. The column was washed with buffer C containing 50 mM imidazole, and recombinant proteins were then eluted using 50–500 mM imidazole gradient in buffer C. The eluted fractions were diluted more than 10-fold into buffer D (50 mM Tris-HCl (pH 7.5), 100 mM NaCl, 2 mM dithiothreitol, 20% (w/v) glycerol) and loaded onto a HiTrap Q column (GE Healthcare). The column was washed with buffer D, and recombinant proteins were eluted using 100–1,000 mM NaCl in buffer D. Each fraction containing recombinant proteins was stored separately at –80 °C.

E. coli cells overproducing glutathione *S*-transferase-fused ClpP (GST-ClpP) were grown at 37 °C in LB medium containing 50 µg/ml ampicillin, and expression of GST-ClpP was induced by the addition of 1 mM IPTG, followed by incubation at 30 °C for 3 h. Cells were harvested and suspended in buffer E (50 mM Tris-HCl (pH 7.4), 10 mM KCl, 10 mM MgCl₂, 1 mM dithiothreitol, 10% (w/v) glycerol). After sonication on ice, cell lysates were centrifuged at 15,000 × *g* for 1 h at 4 °C, and the supernatant was loaded onto a GSTrap HP column (GE Healthcare). The column was washed with buffer E, and recombinant proteins were then eluted with buffer E containing 10 mM reduced glutathione. The eluted fractions containing GST-ClpP were treated with PreScission protease (BD Biosciences) at 4 °C for 12 h to remove a glutathione *S*-transferase moiety. ClpP was further purified by a HiTrap Q column chromatography using 0–500 mM KCl gradient in buffer F (50 mM Tris-HCl (pH 7.5), 2 mM EDTA, 2 mM dithiothreitol, 10% glycerol). Fractions containing ClpP were concentrated with Amicon Ultra-30 (Millipore) and stored at –80 °C.

GFP-SsrA was overexpressed in *E. coli* KY2266 (22). Cells were suspended in buffer G (20 mM Tris-HCl (pH 7.4), 1 mM EDTA) and disrupted by sonication. Subsequently, GFP-SsrA was purified by HiTrap Q column chromatography using 0–1 M NaCl gradient in buffer G. Fractions containing GFP-SsrA were pooled and stored at –80 °C. ClpB was purified as described previously (23).

Protein concentrations were determined by measuring band intensities in SDS-polyacrylamide gels. All protein concentrations are given for protomers.

FtsZ Polymerization Assays—In light scattering assay, FtsZ (12 µM) was preincubated in buffer H (40 mM HEPES-KOH (pH 7.5), 5 mM MgCl₂, 175 mM NaCl, 0.02% Triton X-100, 10% glycerol) at 30 °C for several minutes to correct a base line. Polymerization was started by the addition of 5 mM GTP. Light scattering was continuously recorded every 10 s using a Jasco FP-750 fluorescence spectrophotometer (Jasco Corp.) with both excitation and emission wavelengths set to 500 nm with 5-nm slit widths. Light scattering of ClpX (indicated concentrations) was also monitored with time after the addition of ClpX.

In sedimentation assay, polymerization of FtsZ (6 µM) or FtsZΔC (6 µM) was initiated in buffer H by adding 5 mM GTP. If required, ClpX (6 µM), ClpXΔN (6 µM), ClpX-N (1.5–12 µM), ClpB (6 µM), ClpP (14 µM), SspB (6 µM), and ATP (5 mM) were added. After incubation at 30 °C for 15 min, the reaction was immediately ultracentrifuged at 4 °C in a Beckman TLA 100 rotor (Beckman-Coulter) at 100,000 rpm for 30 min. Processing

ClpX-mediated Inhibition of FtsZ Polymerization

the pellet for protein estimation and SDS-PAGE was performed as described earlier (24). Band intensity on the gel was estimated using ImageQuant (GE Healthcare).

Scanning Electron Microscopy (SEM)—FtsZ polymers were prepared as mentioned above, fixed with 2.5% glutaraldehyde and 2% formaldehyde, placed on a glass slide, and air-dried at room temperature. The samples were coated with platinum and observed using a Keyence VE-9800 scanning electron microscope (Keyence Co.).

High Speed AFM—The laboratory-built tapping mode high speed AFM apparatus, which has been developed by Dr. Ando and co-workers at Kanazawa University (25), was used in this study. The cantilever (Olympus) has a resonant frequency of ~1 MHz in water and a spring constant of 0.1–0.2 newton/m. An amorphous carbon tip was grown on the original cantilever tip by electron beam deposition (26). For high speed AFM observation, FtsZ (6 μM) was incubated in buffer H at 30 °C for 5 min. If required, GTP (5 mM) and ClpX (6 μM) were supplemented. A droplet (2 μl) was deposited on a freshly cleaved mica surface, incubated for 3 min at room temperature, and washed with buffer H. AFM observation was then performed under buffer H minus Triton X-100. ClpX (6 μM) was incubated in buffer I (50 mM Tris-HCl (pH 8.0), 500 mM KCl) at 30 °C for 5 min. A droplet (2 μl) was deposited on a freshly cleaved mica surface, incubated for 3 min at room temperature, and washed with buffer I. AFM observation was then performed under buffer J (40 mM HEPES-KOH (pH 7.4), 150 mM KCl, 20 mM MgCl_2).

Chemical Cross-linking—FtsZ (6 μM) and ClpX (6 μM) were incubated at 30 °C for 10 min in buffer J in the absence and presence of the indicated nucleotides. Proteins were then cross-linked with 0.1% glutaraldehyde at 30 °C for 20 min. The reactions were quenched by the addition of an equal volume of 2 \times SDS sample buffer (150 mM Tris-HCl (pH 6.8), 4% SDS, 20% glycerol, 10% 2-mercaptoethanol). Proteins were analyzed by SDS-PAGE and visualized with Coomassie Brilliant Blue staining. Here, polyacrylamide gradient gels (SuperSep 3–10% gel, Wako) were used to separate proteins with a broad range of molecular masses.

FtsZ Depolymerization Assay—After polymerization of FtsZ (12 μM) and FtsZ ΔC (12 μM) in buffer H supplemented with GTP (5 mM) at 30 °C for 20 min, ClpX (6 μM) was added to the mixture. The reactions were further incubated at 30 °C for 15 min and immediately ultracentrifuged at 4 °C in a Beckman TLA 100 rotor at 100,000 rpm for 30 min. Both supernatant and pellet fractions were analyzed by SDS-PAGE with Coomassie Brilliant Blue staining. The reactions without the addition of ClpX were used as a negative control.

Protein Degradation—FtsZ (3 μM) and GFP-SsrA (3 μM) were degraded by ClpXP (ClpX, 6 μM ; ClpP, 14 μM) in buffer K (25 mM HEPES-KOH (pH 7.6), 100 mM KCl, 20 mM MgCl_2 , 1 mM EDTA) at 30 °C for 120 min. Protein degradation was analyzed by SDS-PAGE with Coomassie Brilliant Blue staining. Estimation of substrate degradation was performed using ImageQuant (GE Healthcare).

Fluorescence Microscopy—*E. coli* MC4100(DE3) (27) was transformed with pET-28b, pET28-ClpX, pET28-ClpX ΔN , or pET28-ClpX-N. These transformants were inoculated to LB

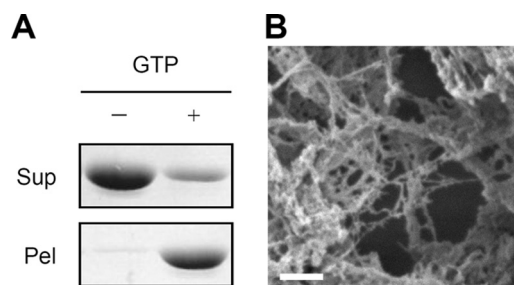


FIGURE 1. GTP-dependent assembly of FtsZ into filaments. *A*, FtsZ (6 μM) was polymerized in the absence (–) and presence (+) of 5 mM GTP and separated by ultracentrifugation into supernatant (*Sup*) and pellet (*Pel*) fractions. FtsZ in each fraction was analyzed by SDS-PAGE and Coomassie Brilliant Blue staining. *B*, SEM image of FtsZ filament is shown. Scale bar is given as 1 μm .

media containing 40 $\mu\text{g/ml}$ kanamycin and cultured at 37 °C overnight. Cell morphologies were observed by fluorescence microscopy with a phase-constant mode. Because leaky expression of ClpX variants was enough to show abnormal morphologies, no IPTG was supplemented into the cultures. To examine the localization of FtsZ, pFtsZ-GFP_{uv} and either pET-28b or pET28-ClpX were simultaneously introduced into *E. coli* MC4100(DE3). These transformants were cultured in LB media containing 40 $\mu\text{g/ml}$ kanamycin and 50 $\mu\text{g/ml}$ ampicillin at 37 °C overnight. As high level FtsZ-GFP_{uv} expression induces filamentous cells, no IPTG was supplemented into the cultures. Cells were then fixed with methanol and stained with 4,6-diamidine-2-phenylindole (DAPI) (28). Localization of FtsZ-GFP_{uv} and nucleoids was observed under fluorescence microscopy with green fluorescent protein and DAPI filters, respectively.

RESULTS

FtsZ Polymerizes into Fibers in the Presence of GTP—GTP-dependent polymerization of purified FtsZ was confirmed by sedimentation assay. In the absence of GTP, almost all FtsZ was retained in the supernatant fraction, although, in the presence of GTP, FtsZ was found predominantly in the pellet fraction (Fig. 1*A*). Kinetics of FtsZ polymerization revealed that FtsZ polymerized immediately after the addition of GTP, and the polymers were stable for at least 30 min under the conditions used (supplemental Fig. S1). Rapid increase in the population of FtsZ polymers is consistent with the result of light scattering analysis (data not shown). We also observed the structure of GTP-induced FtsZ polymers by SEM and detected networks of filaments (Fig. 1*B*) as demonstrated previously by transmission electron microscopy (24).

FtsZ Polymers Undergo Dynamic Conformational Changes—The AFM is a powerful tool to capture high resolution images of biological samples in liquids without any fixation chemicals unlike electron microscopy. However, the conventional AFM takes at least 30–60 s to capture an image, whereas dynamic biomolecular processes occur on a millisecond time scale or less. FtsZ polymers are also known to be in a dynamic equilibrium, and subunits within the polymer are rapidly exchanged on a time scale of 7 s (29). Therefore, it had been impossible to capture the movements of FtsZ polymers by the conventional AFM. Here, we applied a recently developed method, high speed AFM, which enables us to visualize conformational

changes of native proteins directly in solution on much smaller time scales (30–60 ms) (25).

First, we compared AFM images of FtsZ between the presence and absence of GTP. In the absence of GTP, small particles with different shapes were detected (Fig. 2A). Based on the results of chemical cross-linking that FtsZ predominantly formed monomers (data not shown), FtsZ monomers seemed to be adsorbed on mica. In contrast, in the presence of GTP, networks of long filaments containing single straight, curved, and bundled filaments were detected (Fig. 2C). The heights of FtsZ filaments (average 5.2 nm, Fig. 2D) were similar to those of monomers and dimers (average 4.4 nm, Fig. 2B), suggesting that FtsZ monomers and dimers assemble into a single filament by longitudinal interaction.

Next, to ask whether FtsZ polymers undergo dynamic conformational changes, we continuously captured AFM images

with a fast scan rate (~ 1 frame/s). As shown in Fig. 3 and [supplemental Fig. S2](#), we succeeded to detect directly the conformational changes of FtsZ polymers. Some straight filaments gradually curved, and others laterally associated into bundles. Partial dissociation and reassembly of filaments were also detected (Fig. 3 and [supplemental Fig. S2](#)). To our knowledge, this is the first vivid visualization of conformational changes of FtsZ polymers on a second time scale using a high speed AFM.

ClpX Forms Heterogeneous Oligomers—Prior to investigating the effect of ClpX on FtsZ polymerization *in vitro*, we analyzed the oligomeric state of purified ClpX. In the absence of nucleotides, light scattering signal of ClpX increased in a dose-dependent manner (Fig. 4A), indicating that ClpX forms large oligomers under the conditions used.

To investigate the oligomeric state of ClpX in detail, we conducted a glutaraldehyde cross-linking assay. As shown in Fig. 4B, smear bands around the position of dimers and hexamers were predominantly detected in the absence of nucleotides. Interestingly, hexamers were obviously detected in the presence of the nonhydrolyzable analog of ATP, ATP γ S, rather than in the presence of ATP or ADP. In addition, in the presence of nucleotides, the amount of dimer was reduced compared with that in the absence of nucleotides, and large oligomers were concomitantly detected around the position of wells (Fig. 4B). These observations are consistent with a previous report showing that ClpX showed heterogeneously sized particles with no obvious regularity and that the addition of ATP γ S to ClpX produced a more uniform particle with a size corresponding to a hexamer (30).

Structure and size distribution of ClpX molecules were also evaluated by AFM. ClpX was observed as heterogeneous globular particles with a size distribution ranging from 3 to 50 nm in height and 2 to 33 nm in width (Fig. 4C), indicating that ClpX exists as heterogeneously sized particles ranging from a monomer to a large oligomer. The result of chemical cross-linking also showed similar heterogeneous oligomeric states of ClpX (Fig. 4B).

ClpX Inhibits FtsZ Polymerization—Light scattering assay is a useful method to analyze the time course of FtsZ polymerization *in vitro*. However, because ClpX itself shows a large light scattering (Fig. 4A), this method was not employed to investigate the ability of ClpX to modulate the FtsZ assembly. Therefore, we conducted a sedimentation assay and evaluated band intensities of the sedimented FtsZ to quantify the formation of polymers. After polymerization at 30 °C for 15 min, the reaction was centrifuged at 100,000 rpm for 30 min at 4 °C, and the pellet fraction was analyzed by SDS-PAGE. When the amount of polymerized FtsZ in the presence of GTP is defined as 100%, the addition of ClpX to the reaction reduced it to $\sim 20\%$ (Fig. 5, A and B). Surprisingly, ATP slightly but significantly inhibited the activ-

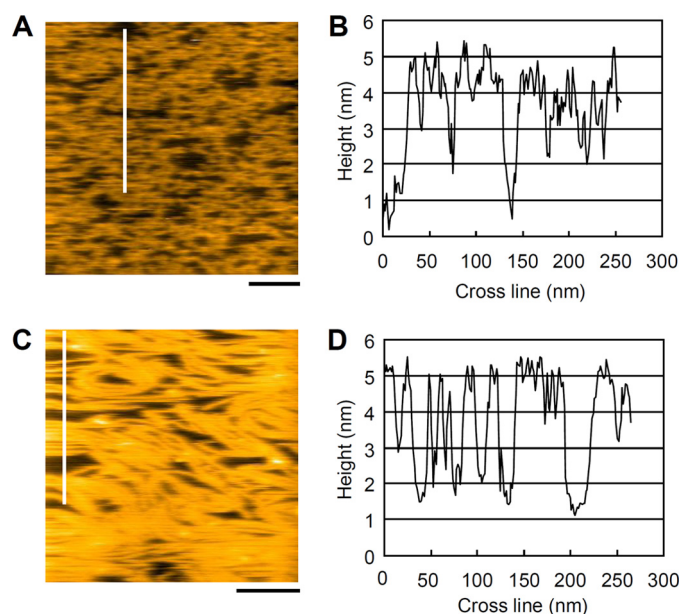


FIGURE 2. AFM images of FtsZ monomers and polymers. A, AFM image of FtsZ in the absence of GTP is shown. B, height of FtsZ at the white-lined cross-section in A was measured. C, AFM image of GTP-triggered FtsZ polymers is given. D, height of FtsZ at the white-lined cross-section in C was measured. Scale bars in A and C are given as 100 nm.

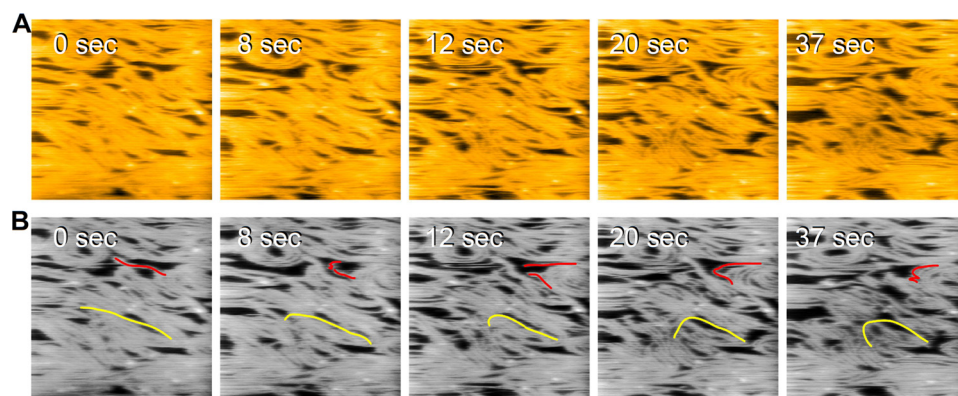


FIGURE 3. High speed AFM images of FtsZ polymers. A, raw AFM images of FtsZ polymers taken at the indicated times. There are many single filaments, bundles, and curved filaments. B, to emphasize the dynamic nature of filaments, raw images in A are shown in gray scale, and selected filaments are colored in red. A straight filament was curved, disassembled, reassembled, and bundled under the observation. Scale bar is given as 100 nm.

ClpX-mediated Inhibition of FtsZ Polymerization

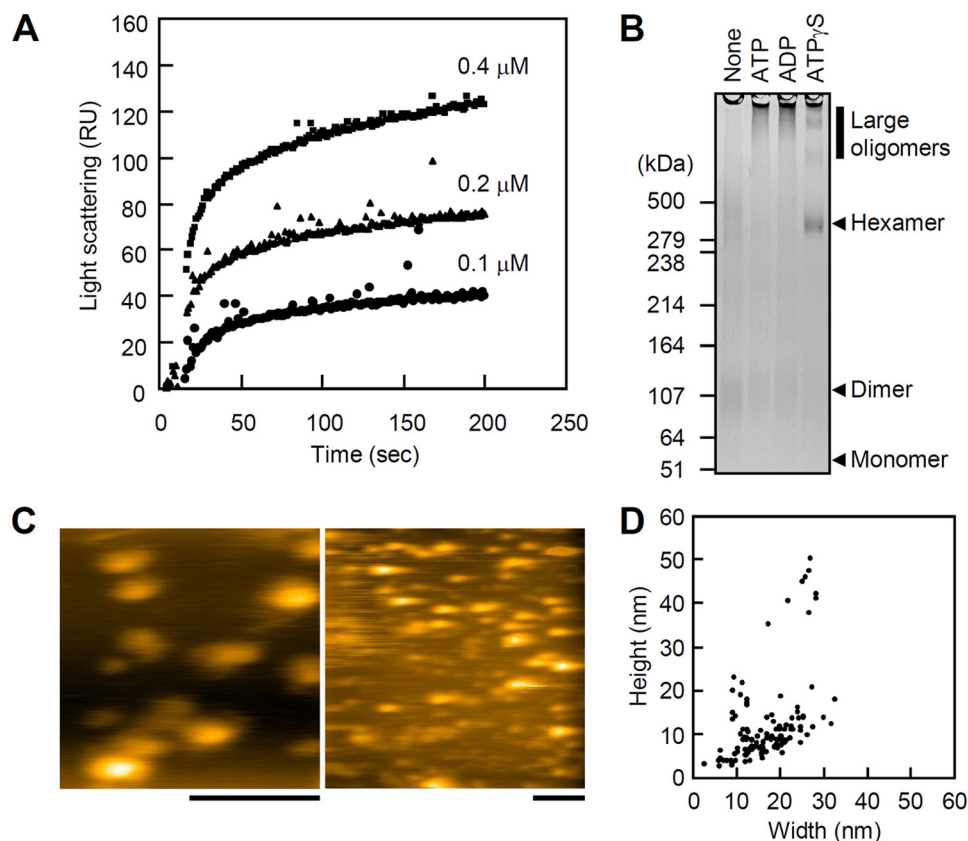


FIGURE 4. Oligomeric state of ClpX. *A*, light scattering of ClpX (indicated concentrations) in the absence of nucleotide was measured as described under "Experimental Procedures." *RU*, response units. *B*, ClpX ($6 \mu\text{M}$) was incubated in the absence and presence of the indicated nucleotides (5 mM) at 30°C for 10 min and then cross-linked with 0.1% glutaraldehyde at 30°C for 20 min. After quenching the reaction by the addition of Tris-HCl-containing buffer, proteins were analyzed by SDS-3–10% gradient polyacrylamide gel. The molecular sizes in kilodaltons are given at the left. The positioning of monomer, dimer, hexamer, and large oligomers is given. *C*, AFM images at two magnifications are shown. Scale bars are given as 100 nm. *D*, width (*x* axis) and height (*y* axis) of ClpX molecules ($n = 120$) in *C* and other frames were measured and plotted.

ity of ClpX to prevent FtsZ polymerization (Fig. 5, *A* and *B*). The addition of ATP did not affect FtsZ polymerization itself. In addition, ATP γ S also reduced the activity of ClpX, although ADP did minimally, indicating that an ATP-bound form of ClpX is ineffective for inhibition of FtsZ polymerization. Thus, henceforth ATP was not added to reactions. To ask whether the effect on FtsZ polymerization is unique for ClpX, the effects of ClpB (another AAA⁺ chaperone), ClpP (protease component of ClpXP), and SspB (adaptor protein of ClpXP) were tested. ClpB, ClpP, and SspB slightly inhibited FtsZ polymerization, but their effects were at negligible levels (Fig. 5*C* and supplemental Fig. S3). These results indicate that FtsZ polymerization is specifically inhibited by ClpX. As SspB, which stimulates degradation of SsrA-tagged substrates by ClpXP (31), did not show significant inhibition of FtsZ assembly, an FtsZ recognition mode of ClpX is distinct from that of SsrA-tagged substrates by ClpX and SspB.

To examine how ClpX prevents FtsZ polymerization, structures of FtsZ were visualized by AFM. In the presence of GTP, many filamentous structures were detected as shown in Figs. 2*C*, 3, and 5*D*. In the simultaneous presence of GTP and ClpX, no obvious long filament was detected, but small particles were observed (Fig. 5*D*). Here, ClpX dimers and FtsZ monomers/dimers were not distinguishable. Taking into consideration

that no obvious filament was detected, ClpX inhibits the longitudinal assembly of FtsZ at the initial step, in which binding of FtsZ protomers occurs.

N-terminal Domain of ClpX Plays a Crucial Role in the Inhibition of FtsZ Polymerization—N-terminal domains of several AAA⁺ chaperones are known to function in the substrate recognition and to act as a primary binding site. The N-terminal domain of ClpX also plays a crucial role in the recognition of specific target proteins, including MuA and λ O (4). In contrast, it does not play a role for the recognition of some other substrates such as GFP-SsrA (4). To address whether the N-terminal domain of ClpX is involved in the recognition of FtsZ, we generated a ClpX mutant, ClpX Δ N, lacking the N-terminal domain and examined its effect on FtsZ polymerization (Fig. 5*C*). Compared with wild type ClpX, ClpX Δ N showed very weak inhibition, suggesting that the N-terminal domain is responsible for the recognition of FtsZ. A recent report revealed that ClpX Δ N, together with ClpP, showed a reduced but still significant ability to degrade FtsZ (21), suggesting that the AAA⁺

domain of ClpX has a weak ability to recognize and unfold FtsZ.

To examine the possibility that the N-terminal domain of ClpX has the capacity to bind to FtsZ and to inhibit FtsZ polymerization, we constructed and purified a ClpX mutant, ClpX-N, composed of the N-terminal domain. ClpX-N critically inhibited FtsZ polymerization in a dose-dependent manner (Fig. 5*E*), suggesting that the N-terminal domain of ClpX plays a primary role in the regulation of FtsZ dynamics and that the AAA⁺ domain is not essential for this function. It is interesting to mention that when the reactions were conducted with the same concentrations of ClpX-N and ClpX ($6 \mu\text{M}$ as monomers), ClpX-N showed a stronger inhibitory effect on FtsZ polymerization than did ClpX (Fig. 5, *B* and *E*). This is likely due to differences in the number of N-terminal domains accessible for FtsZ, which might be limited by formation of hexamers and oligomers in the case of ClpX (Fig. 4*B*).

ClpX Recognizes a C-terminal Moiety and Other Parts of FtsZ—The C-terminal unstructured region of FtsZ (residues 328–383) is recognized by several FtsZ modulators, such as FtsA, MinC, and ZipA (15–17). Furthermore, it has recently been reported that this region is important for degradation of FtsZ by ClpXP (21). To ask whether the C-terminal region of FtsZ is essential for the inhibition of FtsZ polymerization by ClpX, we generated an FtsZ mutant, FtsZ Δ C, lacking the C-terminal res-

ClpX-mediated Inhibition of FtsZ Polymerization

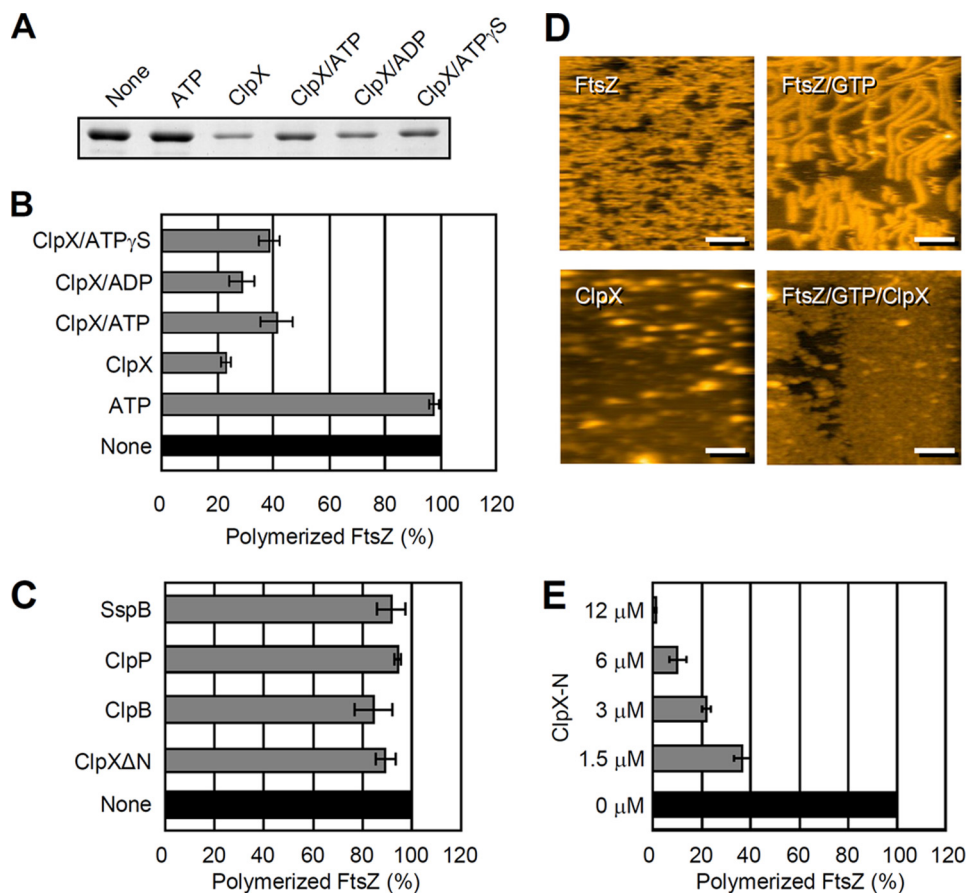


FIGURE 5. Inhibition of FtsZ polymerization by ClpX. *A*, FtsZ (6 μ M) was polymerized in the presence of GTP with or without ClpX and the indicated nucleotides. FtsZ polymers were collected by ultracentrifugation and analyzed by SDS-PAGE. *B*, band intensities of FtsZ polymers in *A* were quantified as described under “Experimental Procedures.” *C*, degrees of GTP-induced FtsZ polymers formed in the absence and presence of the indicated chaperones (6 μ M per monomer) are given. *D*, inhibition of FtsZ polymerization by ClpX is visualized by AFM. AFM images of FtsZ, in the absence and presence of GTP, and ClpX are also shown. All scale bars are given as 100 nm. *E*, dose dependence of ClpX-N in inhibition of FtsZ assembly is examined. The indicated monomer concentrations of ClpX-N were added to the FtsZ polymerization reaction. *B*, *C*, and *E*, level of FtsZ polymers formed in the presence of GTP was defined 100%. All polymerization reactions were started by the addition of 5 mM GTP. Data from at least three replicates are presented as means \pm S.E.

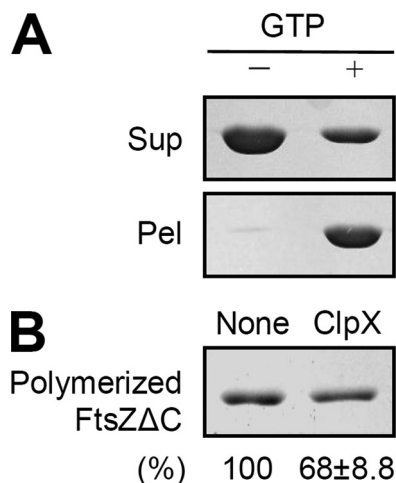


FIGURE 6. Inhibition of GTP-dependent polymerization of FtsZ Δ C. *A*, GTP-dependent polymerization of FtsZ Δ C was confirmed as shown in Fig. 1*A*. *Sup*, supernatant; *Pel*, pellet. *B*, inhibition of FtsZ Δ C polymerization by ClpX was examined as shown in Fig. 5*A*. The quantified values of FtsZ Δ C polymers in the absence and presence of ClpX are indicated at the bottom. Data from at least three replicates are presented as means \pm S.E.

idues 317–383. FtsZ Δ C polymerized in the presence of GTP (Fig. 6*A*) similarly to wild type FtsZ (Fig. 1*A*). Polymerization of FtsZ Δ C was inhibited by ClpX (Fig. 6*B*). Compared with the case of wild type FtsZ (Fig. 5, *A* and *B*), the level of ClpX-mediated inhibition of FtsZ Δ C polymerization was markedly low (Fig. 6*B*), indicating that the C-terminal region of FtsZ has a substantial role for the recognition by ClpX, but it is not essential for the inhibition of FtsZ polymerization.

ClpX Blocks Reassembly of FtsZ Polymers—Because FtsZ is in a dynamic equilibrium between polymerization and depolymerization as shown by high speed AFM (Fig. 3 and supplemental Fig. S2), we assumed that ClpX can affect the oligomeric state of preformed FtsZ polymers. The FtsZ polymers were formed in the presence of GTP at 30 $^{\circ}$ C and then incubated with ClpX as described under “Experimental Procedures.” As expected, ClpX significantly reduced the amount of FtsZ polymers as well as FtsZ Δ C polymers (Fig. 7), showing again that the C-terminal region of FtsZ is not required for the ClpX-mediated inhibition of FtsZ reassembly as in the case of the prevention of the initial step of FtsZ assembly (Fig. 5). It should be emphasized that no energy of ATP hydrolysis was

required for this reaction, indicating that binding to FtsZ is enough to block the assembly and reassembly of FtsZ and that this activity does not contain an energy-consuming process such as protein unfolding and translocation.

ClpX Slightly Unfolds FtsZ—Recently, it has been reported that *E. coli* ClpXP degraded FtsZ more rapidly in the presence than in the absence of GTP, suggesting that ClpXP preferentially degrades FtsZ polymers rather than monomers (21). In addition, ClpX-mediated inhibition of FtsZ polymerization was not observed (21). Based on these results, they proposed that ClpXP may participate in cell division by modulating the equilibrium between monomeric and polymeric FtsZ via degradation of FtsZ polymers. In contrast, it has been reported that in *B. subtilis* ClpXP does not degrade FtsZ and that ClpX regulates FtsZ polymer dynamics by preventing FtsZ polymerization (19). Our present results mentioned above are consistent with the latter result, but contribution of FtsZ degradation (or unfolding) by ClpXP (or ClpX) to the regulation of FtsZ polymer dynamics remains to be elucidated. Therefore, we reassessed FtsZ degradation by ClpXP using *E. coli* proteins.

ClpX-mediated Inhibition of FtsZ Polymerization

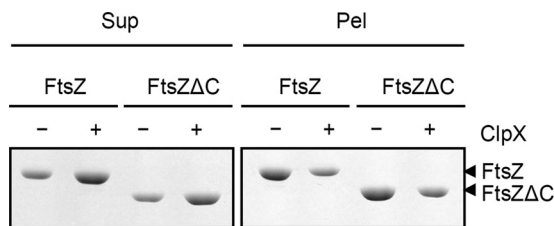


FIGURE 7. Depolymerization of FtsZ polymers mediated by ClpX. FtsZ and FtsZ Δ C (12 μ M each) were polymerized by the addition of GTP and then unsupplemented (-) or supplemented (+) with ClpX. After the depolymerization reaction, depolymerized (and/or unpolymerized) and polymerized FtsZ was separated by ultracentrifugation and analyzed by SDS-PAGE as described under "Experimental Procedures." The positioning of FtsZ and FtsZ Δ C is given. *Sup*, supernatant; *Pel*, pellet.

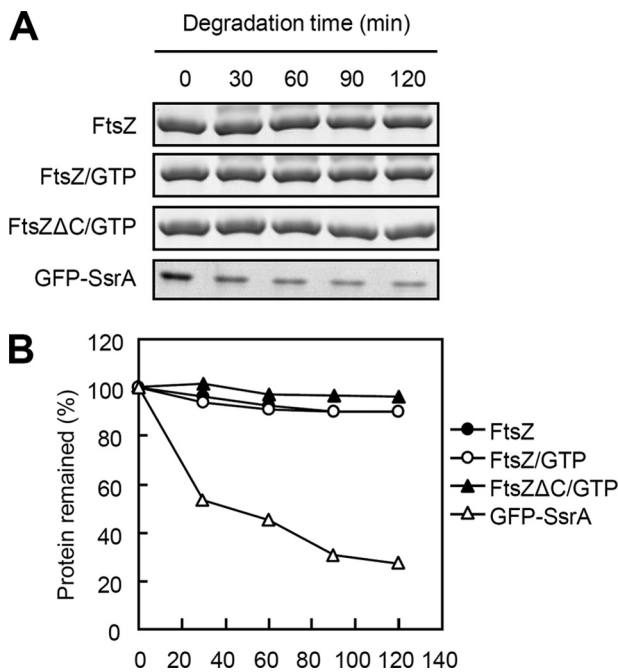


FIGURE 8. Degradation of FtsZ by ClpXP. *A*, FtsZ monomers, preferentially formed in the absence of GTP (closed circles), and polymers, preferentially formed in the presence of GTP (open circles), were degraded by ClpXP for 120 min. To address the importance of C-terminal region, FtsZ Δ C (closed triangles) was also analyzed. As positive controls, GFP-SsrA (open triangles) was degraded by ClpXP in the absence of GTP. At the indicated times, an aliquot of each reaction was taken and analyzed by SDS-PAGE. *B*, band intensities of the substrate proteins were quantified using ImageQuant.

As shown in Fig. 8, ClpXP showed a weak activity to degrade FtsZ. The degradation rate of FtsZ was \sim 2-fold faster than that of FtsZ Δ C, indicating that the C-terminal region of FtsZ is important for the proteolysis by ClpXP as recently reported (21). However, the rate of FtsZ degradation in the presence of GTP, the condition favoring polymers, was similar to that in the absence of GTP, the condition favoring monomers; this is inconsistent with the results of Camberg *et al.* (21). Although the reason for this discrepancy is unclear, it might be due to the difference in the experimental conditions and the methods to detect the degradation of FtsZ. More importantly, the degradation of FtsZ by ClpXP (10% degradation in 2 h) was quite slower than that of GFP-SsrA (80% degradation in 2 h) under the conditions used (Fig. 8), suggesting that contribution of FtsZ unfolding by ClpX to the inhibition of FtsZ polymerization by ClpX is a negligible level (15-min incubation, Fig. 5, *A* and *B*).

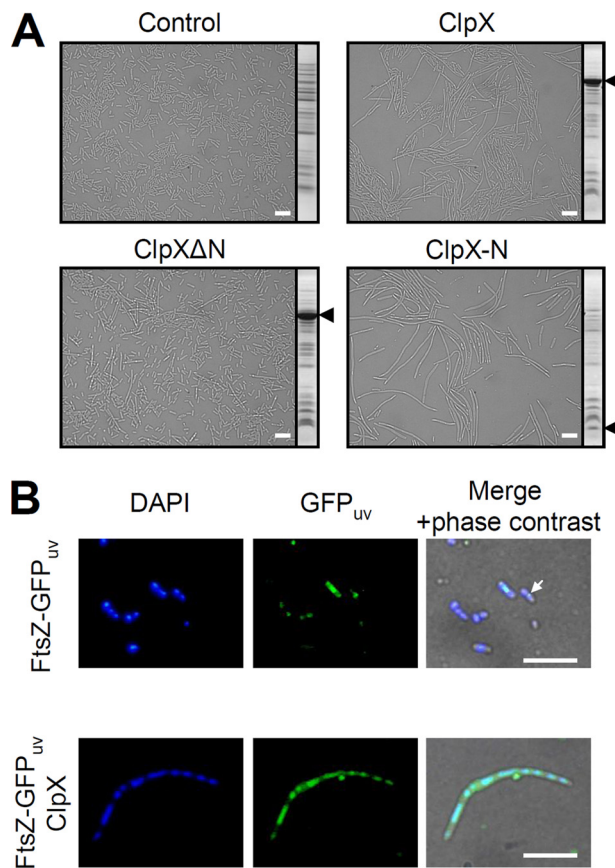


FIGURE 9. Effects of ClpX overexpression on *E. coli* cell morphology and Z-ring formation. *A*, cell morphologies of vector control (*Control*), ClpX-overexpressing (*ClpX*), ClpX Δ N-overexpressing (*ClpX Δ N), and ClpX-N-overexpressing (*ClpX*-N) cells are shown. Protein expression profile of each transformant is analyzed by SDS-PAGE with Coomassie Brilliant Blue staining and attached to the right of each panel. An arrowhead indicates the position corresponding to each overexpressed protein. *B*, to visualize localization of FtsZ, the FtsZ-GFP_{uv} expression plasmid was cotransformed with the empty plasmid or ClpX-expression plasmid into *E. coli* MC4100(DE3). DNA was stained with DAPI. Fluorescence of DAPI and GFP_{uv} was captured by fluorescent microscopy with the respective filters. Merged pictures of DAPI, GFP_{uv}, and phase contrast are also shown. A significant Z-ring is indicated by an arrow. All scale bars are given as 10 μ m.*

Overexpression of ClpX Induces Cell Division Defect and Inhibits Z-ring Formation—Because normal assembly and localization of FtsZ are deeply related to correct cell division (32), we examined the effect of ClpX overexpression on the cell division and Z-ring formation in *E. coli* (Fig. 9). Cells harboring a vector showed typical rod shape, whereas ClpX-overexpressing cells showed many filaments (Fig. 9A), indicating that overexpression of ClpX leads to the defect in cell division. Next, we investigated the effect of overexpression of ClpX variants, including ClpX Δ N and ClpX-N. ClpX Δ N-overexpressing cells showed some elongated cells, but rod-type cells were mainly observed (Fig. 9A). The difference of cell morphology between ClpX-overexpressing and ClpX Δ N-overexpressing cells was not due to the different expression levels, because similar amounts of these proteins were detected by SDS-PAGE. In contrast, ClpX-N-overexpressing cells showed long filaments (Fig. 9A), suggesting that the reason ClpX overexpression leads to cell division defect is not the depletion of endogenous FtsZ by proteolytic activity of ClpXP. In addition, only a few elongated cells were observed when ClpB and SspB were overex-

pressed (supplemental Fig. S4). These results of the *in vivo* experiments are highly consistent with those of the *in vitro* experiments (Fig. 5).

Next, to check the Z-ring formation *in vivo*, we introduced two plasmids to express ClpX and FtsZ-GFP_{uv} into *E. coli* cells. This enables us to visualize the localization of FtsZ *in vivo*. Without ClpX overexpression, typical rod cells with the proper Z-ring were detected. In contrast, when ClpX was overexpressed, no Z-ring was observed in filamentous cells (Fig. 9B). Note that almost all FtsZ colocalized with nucleoid because of unknown reasons. Taken together, these results indicate that overexpression of ClpX inhibits the assembly of FtsZ *in vivo*, leading to defective cell division.

DISCUSSION

Here, we examined molecular mechanisms of remodeling of *E. coli* cell division protein FtsZ by AAA⁺ chaperone ClpX. We observed that ClpX shifts the dynamic equilibrium of FtsZ from polymers toward monomers, working at the initial step of FtsZ assembly. In this function, the N-terminal domain of ClpX plays a crucial role in the recognition and remodeling of FtsZ *in vitro* and *in vivo*. A C-terminal region of FtsZ in part contributes to inhibition of FtsZ polymerization by ClpX as well as degradation of FtsZ by ClpXP.

High Speed AFM Is a Superior Method for Visualizing FtsZ Filament Dynamics—In this study, we used a high speed AFM to visualize FtsZ polymer dynamics on second time scales. Previously, it has been reported that single FtsZ filament dynamics were visualized with an AFM taking images every 2 min (14). However, because the time scale of FtsZ filament dynamics is much shorter than 2 min (29), an AFM with higher time resolution was desired to visualize FtsZ filament dynamics. Using a high speed AFM, we found that FtsZ is in a dynamic equilibrium between monomers and polymers and that those FtsZ polymers undergo dynamic conformational changes such as curvature and bundling (Fig. 3 and supplemental Fig. S2). Previous reports suggested that curvature (12) and depolymerization of FtsZ filaments (8, 9) are triggered by GTP hydrolysis from experimental data with nucleotide analogs. In contrast, a recent study demonstrated that formation of curved filaments is independent of GTP hydrolysis (14). Although mechanisms of conformational changes of FtsZ driven by GTP binding and hydrolysis are still unclear (33), our present approach using a high speed AFM has the great potential to provide novel insights into dynamics of GTP-dependent assembly and conformational changes of FtsZ. We are now trying to visualize the initial process of FtsZ polymerization, ClpX-mediated FtsZ depolymerization, and ClpXP-mediated FtsZ degradation.

Effect of ATP on ClpX Activity to Regulate FtsZ Polymer Dynamics—Previously, it has been reported that ATP binding but not ATP hydrolysis enhances the activity of *B. subtilis* ClpX to inhibit FtsZ polymerization, because the addition of ATP, ADP, and ATP γ S equally exhibited positive effects on it (19). Recently, by the same group it has been reported that a ClpX mutant (E182A), which is defective in the ATP hydrolysis, showed a reduced ability to inhibit FtsZ polymerization *in vitro*, and thus it has been speculated that ATP hydrolysis is required for maximum inhibition (20). Therefore, the significance of

ATP hydrolysis remains to be elucidated. Based on the previous finding that at least ATP binding has a role for modulation of the ClpX activity (19), they expected that ATP binding triggers the hexamer formation of ClpX, leading to a maximum activity of ClpX. However, they did not show the oligomeric state of *B. subtilis* ClpX under the conditions tested. More importantly, if ATP affects the oligomer formation of ClpX, light scattering assay is not available to evaluate FtsZ polymerization in the presence of ClpX, because ClpX oligomerization and the formation of complexes between FtsZ and ClpX severely affect light scattering signal of FtsZ polymers. Therefore, we alternatively employed a sedimentation assay in this study.

We found that the N-terminal domain of ClpX has a major role for regulating FtsZ polymer dynamics *in vitro* and *in vivo* (Figs. 5 and 9). This is highly correlated with the finding that, for inhibition of FtsZ polymerization, ClpX does not require ATP and energy-consuming steps such as protein unfolding and translocation (Fig. 5) (19). Surprisingly, ATP and ATP γ S reduced the ability of ClpX to inhibit FtsZ polymerization (Fig. 5); this is inconsistent with the previous report by Weart *et al.* (19). Based on our data with *E. coli* proteins, we propose a possible explanation for the effect of ATP on ClpX activity to inhibit FtsZ assembly; ATP binding induces conformational changes of ClpX leading to unsuitable structures of the N-terminal domain of ClpX for binding to FtsZ. Actually, binding and/or hydrolysis of ATP in the AAA⁺ domain of ClpX induces a large movement of the N-terminal domain (34). Because the N-terminal domain of ClpX forms dimers (4) and has the ability to inhibit the FtsZ assembly, large oligomer formation in the presence ATP or stable hexamer formation in the presence of ATP γ S (Fig. 4) would lead to the reduction of the freely accessible N-terminal domain of ClpX. A recent finding that a mutation into the Walker B motif (E182A) reduced the ClpX activity to inhibit FtsZ assembly *in vitro* (20) can also be accounted for by our proposed molecular mechanism, because the ATP hydrolysis mutant, ClpX (E182A), might be kept in a state of ATP-bound hexamer. Taking into consideration that the negative effect of ADP was smaller than that of ATP and ATP γ S, the ADP-bound but not ATP-bound ClpX is in a preferred conformation for FtsZ recognition.

ClpX Recognizes the C Terminus and Other Parts of FtsZ—To date, several FtsZ modulators have been identified in *E. coli*. MinC, one of the negative regulators for FtsZ assembly, recognizes a C-terminal unstructured region of FtsZ (supplemental Fig. S5) (17). FtsA and ZipA, which collaborate in anchoring FtsZ to membrane and stabilize the Z-ring, also interact with the C-terminal region of FtsZ (supplemental Fig. S5) (15, 16). SulA, a cell division inhibitor of the SOS response that prevents FtsZ assembly and facilitates FtsZ depolymerization, interacts with the C-terminal domain of FtsZ (supplemental Fig. S5) (18). In the case of FtsZ degradation by ClpXP, the C-terminal unstructured region of FtsZ is important for the recognition by ClpX (Fig. 10) (21). Similarly, the C-terminal region of FtsZ acts as a recognition signal for the inhibition of FtsZ polymerization by ClpX (Fig. 7), but other parts of FtsZ are also recognized by the N-terminal domain of ClpX. Previously, it has been reported that the N-terminal domain of ClpX preferentially recognizes several signal sequences containing hydrophobic

ClpX-mediated Inhibition of FtsZ Polymerization

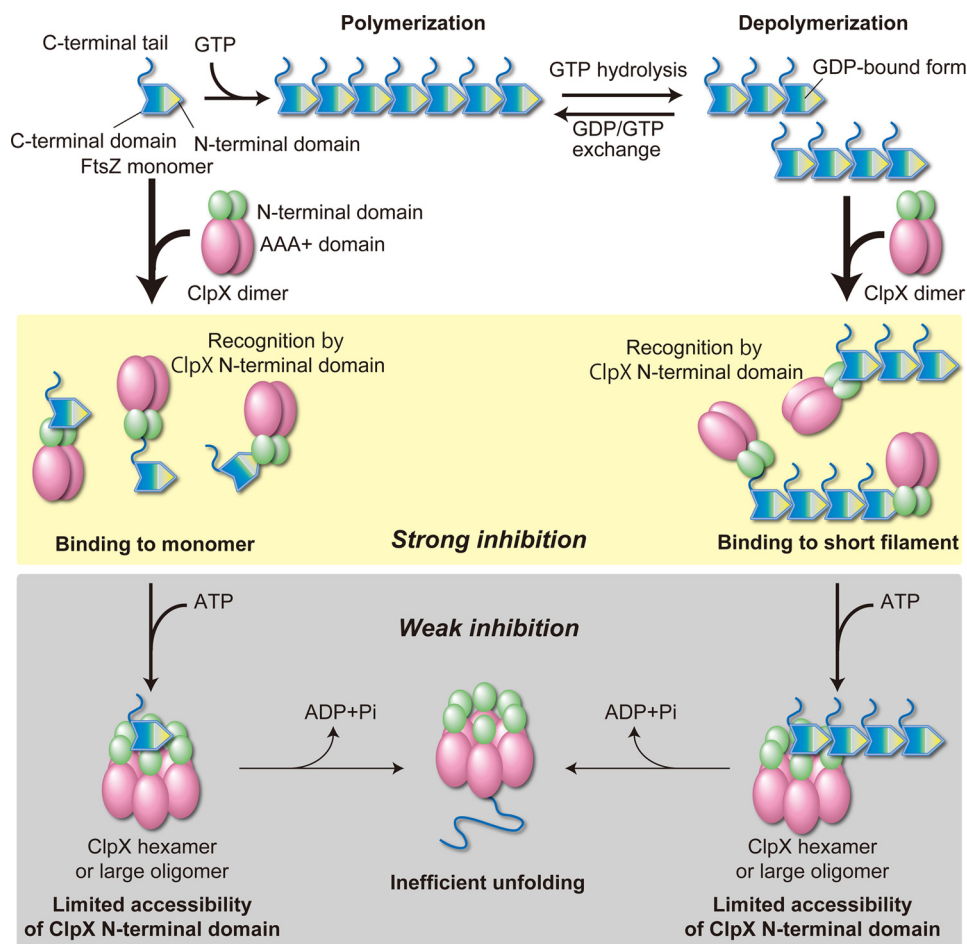


FIGURE 10. Proposed molecular mechanisms for the remodeling of FtsZ polymer dynamics by ClpX. FtsZ is in GTP-dependent polymer dynamics. GTP binding triggers FtsZ polymerization, whereas hydrolysis or release of GTP induces depolymerization. Reassembly of the disassembled FtsZ filaments and/or monomers is induced by GDP/GTP exchange or GTP rebinding. ClpX binding to FtsZ monomers or short polymers results in prevention of assembly and reassembly of FtsZ. In the absence of ATP, ClpX predominantly forms dimers or small oligomers, and many N-terminal domains of ClpX seem to be accessible for FtsZ. Therefore, strong inhibition of FtsZ polymerization is archived. In the presence of ATP, ClpX forms hexamers or more large oligomers. Some of them can slightly unfold FtsZ monomers or polymers by using the energy from ATP hydrolysis, but its contribution to prevention of FtsZ assembly would be a negligible level. Alternatively, FtsZ-accessible N-terminal domains in ClpX hexamers and large oligomers are limited, and thus inhibition of FtsZ polymerization is weakened.

residues (34). Based on their results, we searched for ClpX recognition signals in FtsZ and found several candidates (supplemental Fig. S5). When the sequences buried inside the folded structure are eliminated, we identified only three sequences (supplemental Fig. S5). Interestingly, all of them are located in the structures forming binding interfaces between FtsZ protomers. It is therefore reasonable to speculate that ClpX recognizes one or more regions facing toward neighbor protomers.

Action of ClpX toward Preformed FtsZ Polymers—Interestingly, we found that ClpX can act on preformed FtsZ polymers (Fig. 7). Based on the current finding that FtsZ is in a dynamic equilibrium between monomers and polymers (Fig. 3 and supplemental Fig. S2), ClpX seems to inhibit reassembly of FtsZ monomers and short filaments rather than to disassemble or sever FtsZ polymers. In eukaryotes, it has been shown that AAA family proteins Spastin and Katanin disassemble and sever taxol-stabilized microtubules, the polymer of α/β -tubulin

dimers, *in vitro* (35, 36). However, taking into consideration that tubulins are also in a dynamic equilibrium between monomers and polymers (37) like FtsZ, Spastin and Katanin may have the potential to shift the equilibrium toward monomers from polymers by inhibiting assembly and reassembly of α/β -tubulin dimers in a manner similar to ClpX-mediated inhibition of FtsZ polymerization. Recently, we have reported that the N terminus followed by the AAA domain of SPAS-1, the Spastin homolog in *Caenorhabditis elegans*, interacts with α/β -tubulin dimers (38). It is interesting to mention that the effect of AAA⁺ protein on the protein polymerization has been demonstrated by using yeast prion polymers. Both *in vivo* and *in vitro* data suggest that Hsp104 disassembles amyloid-like aggregates of Sup35, Ure2, and Rnq1 (39–41). Importantly, similar to our findings, these effects of Hsp104 are also modulated by its N-terminal domain (42).

Molecular Mechanisms for the Remodeling of FtsZ Polymer Dynamics by ClpX—Based on our data, we propose molecular mechanisms for the remodeling of FtsZ polymer dynamics by ClpX (Fig. 10). FtsZ is in a dynamic equilibrium between monomers and polymers (Fig. 3 and supplemental Fig. S2), which is triggered by GTP binding/hydrolysis and GDP/GTP exchange. In the absence of ATP, ClpX forms

predominantly dimers (Fig. 4) and binds to FtsZ monomers or small oligomers. The binding is achieved by the interaction between the N-terminal domain of ClpX and the C-terminal domain and other parts of FtsZ. Importantly, an effective inhibition of FtsZ polymerization is provided only by binding of ClpX with FtsZ. Similarly, ClpX interacts with spontaneously depolymerized FtsZ, including a variety of oligomeric structures ranging from monomers to small oligomers, and subsequently it prevents reassembly of them. If FtsZ assembly is unidirectional, ClpX binding to either end of FtsZ filament is enough to inhibit the short filament reassembly. In contrast, if it is bidirectional, binding to both ends is required for strong inhibition. In the presence of ATP, ClpX unfolds FtsZ monomers, but the efficiency of FtsZ unfolding by ClpX is very low. Alternatively, ClpX forms hexamers and large oligomers (Fig. 4), and hence, freely accessible N-terminal domains of ClpX are limited, resulting in a decrease in the ClpX activity to suppress FtsZ polymerization.

Acknowledgments—We acknowledge Dr. T. Okuno for FtsZ preparations; Dr. B. Bukau and Dr. S. Hishida for providing plasmids; Dr. K. Sonomoto and S. Matsumoto for sending bacterial strains; Dr. A. Nagafuchi and Dr. T. Seki for SEM operation; Dr. D. Yamamoto for technical advice regarding high speed AFM; Dr. M. Wachi for stimulating discussions, and C. Ichinose for secretarial assistance.

REFERENCES

1. Tucker, P. A., and Sallai, L. (2007) *Curr. Opin. Struct. Biol.* **17**, 641–652
2. Flynn, J. M., Neher, S. B., Kim, Y. I., Sauer, R. T., and Baker, T. A. (2003) *Mol. Cell* **11**, 671–683
3. Martin, A., Baker, T. A., and Sauer, R. T. (2008) *Nat. Struct. Mol. Biol.* **15**, 1147–1151
4. Wojtyra, U. A., Thibault, G., Tuite, A., and Houry, W. A. (2003) *J. Biol. Chem.* **278**, 48981–48990
5. Goehring, N. W., and Beckwith, J. (2005) *Curr. Biol.* **15**, R514–R526
6. Margolin, W. (2005) *Nat. Rev. Mol. Cell Biol.* **6**, 862–871
7. Adams, D. W., and Errington, J. (2009) *Nat. Rev. Microbiol.* **7**, 642–653
8. Mukherjee, A., and Lutkenhaus, J. (1994) *J. Bacteriol.* **176**, 2754–2758
9. Bramhill, D., and Thompson, C. M. (1994) *Proc. Natl. Acad. Sci. U.S.A.* **91**, 5813–5817
10. Romberg, L., Simon, M., and Erickson, H. P. (2001) *J. Biol. Chem.* **276**, 11743–11753
11. Yu, X. C., and Margolin, W. (1997) *EMBO J.* **16**, 5455–5463
12. Lu, C., Reedy, M., and Erickson, H. P. (2000) *J. Bacteriol.* **182**, 164–170
13. Beuria, T. K., Krishnakumar, S. S., Sahar, S., Singh, N., Gupta, K., Meshram, M., and Panda, D. (2003) *J. Biol. Chem.* **278**, 3735–3741
14. Mingorance, J., Tadros, M., Vicente, M., González, J. M., Rivas, G., and Vélez, M. (2005) *J. Biol. Chem.* **280**, 20909–20914
15. Ma, X., and Margolin, W. (1999) *J. Bacteriol.* **181**, 7531–7544
16. Hale, C. A., Rhee, A. C., and de Boer, P. A. (2000) *J. Bacteriol.* **182**, 5153–5166
17. Shen, B., and Lutkenhaus, J. (2009) *Mol. Microbiol.* **72**, 410–424
18. Cordell, S. C., Robinson, E. J., and Lowe, J. (2003) *Proc. Natl. Acad. Sci. U.S.A.* **100**, 7889–7894
19. Weart, R. B., Nakano, S., Lane, B. E., Zuber, P., and Levin, P. A. (2005) *Mol. Microbiol.* **57**, 238–249
20. Haeusser, D. P., Lee, A. H., Weart, R. B., and Levin, P. A. (2009) *J. Bacteriol.* **191**, 1986–1991
21. Camberg, J. L., Hoskins, J. R., and Wickner, S. (2009) *Proc. Natl. Acad. Sci. U.S.A.* **106**, 10614–10619
22. Kanemori, M., Nishihara, K., Yanagi, H., and Yura, T. (1997) *J. Bacteriol.* **179**, 7219–7225
23. Woo, K. M., Kim, K. I., Goldberg, A. L., Ha, D. B., and Chung, C. H. (1992) *J. Biol. Chem.* **267**, 20429–20434
24. Mukherjee, A., and Lutkenhaus, J. (1998) *EMBO J.* **17**, 462–469
25. Ando, T., Kodera, N., Takai, E., Maruyama, D., Saito, K., and Toda, A. (2001) *Proc. Natl. Acad. Sci. U.S.A.* **98**, 12468–12472
26. Ando, T., Uchihashi, T., Kodera, N., Yamamoto, D., Miyagi, A., Taniguchi, M., and Yamashita, H. (2008) *Pflugers Arch.* **456**, 211–225
27. Sugimoto, S., Higashi, C., Saruwatari, K., Nakayama, J., and Sonomoto, K. (2007) *FEBS Lett.* **581**, 2993–2999
28. Hiraga, S., Ichinose, C., Niki, H., and Yamazoe, M. (1998) *Mol. Cell* **1**, 381–387
29. Chen, Y., and Erickson, H. P. (2005) *J. Biol. Chem.* **280**, 22549–22554
30. Grimaud, R., Kessel, M., Beuron, F., Steven, A. C., and Maurizi, M. R. (1998) *J. Biol. Chem.* **273**, 12476–12481
31. Levchenko, I., Seidel, M., Sauer, R. T., and Baker, T. A. (2000) *Science* **289**, 2354–2356
32. Sugimoto, S., Saruwatari, K., Higashi, C., and Sonomoto, K. (2008) *Microbiology* **154**, 1876–1885
33. Oliva, M. A., Cordell, S. C., and Löwe, J. (2004) *Nat. Struct. Mol. Biol.* **11**, 1243–1250
34. Thibault, G., Yudin, J., Wong, P., Tsitrin, V., Sprangers, R., Zhao, R., and Houry, W. A. (2006) *Proc. Natl. Acad. Sci. U.S.A.* **103**, 17724–17729
35. McNally, F. J., and Vale, R. D. (1993) *Cell* **75**, 419–429
36. Roll-Mecak, A., and Vale, R. D. (2008) *Nature* **451**, 363–367
37. Kueh, H. Y., and Mitchison, T. J. (2009) *Science* **325**, 960–963
38. Matsushita-Ishiodori, Y., Yamanaka, K., Hashimoto, H., Esaki, M., and Ogura, T. (2009) *Genes Cells* **14**, 925–940
39. Chernoff, Y. O., Lindquist, S. L., Ono, B., Inge-Vechtomov, S. G., and Liebman, S. W. (1995) *Science* **268**, 880–884
40. Shorter, J., and Lindquist, S. (2004) *Science* **304**, 1793–1797
41. Tipton, K. A., Verges, K. J., and Weissman, J. S. (2008) *Mol. Cell* **32**, 584–591
42. Hung, G. C., and Masison, D. C. (2006) *Genetics* **173**, 611–620